

ENHANCED SOLAR ENERGY ABSORPTION ON NITROGEN-DOPED CARBON NANOTUBES DECORATED WITH GOLD-PALLADIUM BIMETALLIC NANOPARTICLES

by

**Lingling WANG^{a,b}, Guihua ZHU^{a,b}, Long SHEN^c, Wei YU^{a,b*}, Dahai ZHU^{a,b},
Yingchun ZHANG^{a,b}, Liye ZHANG^{a,b}, and Huaqing XIE^{a,b}**

^a School of Environment and Materials Engineering, College of Engineering,
Shanghai Polytechnic University, Shanghai, China

^b Shanghai Innovation Institute for Materials, Shanghai, China

^c Shanghai Shanshan Technology Co., Ltd., Shanghai, China

Original scientific paper

<https://doi.org/10.2298/TSCI170620055W>

Gold-palladium alloy nanoparticles decorated on nitrogen-doped carbon nanotubes (Au-Pd/N-CNT) were prepared by using polyethylene imine reduction method. Polyethylene acts as not only a stabilizing agent, but also a reducing agent, leading to nucleation and growth of nanoparticles on the N-CNT surfaces. All the N-CNT-based nanofluids show broadband absorption across the visible region and near infrared region. The Au-Pd/N-CNT nanofluids absorb more solar irradiation compared with monometallic Pd/N-CNT or Au/N-CNT nanofluid. The photo-thermal conversion efficiency of Au-Pd/N-CNT nanofluids is 62.3%, compared with 53.3% and 57% for Pd/N-CNT and Au/N-CNT, respectively. This enhancement was mainly due to the synergetic effects of N-CNT and Au-Pd alloy nanoparticles.

Key words: *nitrogen-doped carbon nanotubes, solar thermal, plasmonic nanoparticles, photo-thermal conversion*

Introduction

Efficient solar-to-chemical energy conversion is particularly fascinating since the Sun is a promising, clean and abundant source of renewable energy source [1]. Solar energy utilization technologies have been focus on photo-thermal, photo-voltaic, and photo-chemical fields. Photo-thermal utilization can be applied in many areas, such as water heating, power generation, and some other industrial processes [2, 3]. In order to overcome the low efficiency caused by heating the whole fluid volume in photo-thermal conversion, the idea of nanofluids was proposed and first used by Choi [4, 5].

In recent years, a new concept of plasmonic nanofluids based on localized surface plasmon resonance (LSPR) metal nanoparticles (NP) such as Au, Ag, and Cu and the use of nanofluids has been proposed, which arouse the interests of many researchers in an area of Sun to heat conversion [6, 7]. The light absorption of plasmonic metallic NP originates from a collective oscillation of the conduction electrons, which can significantly enhance the light absorption and scattering [8, 9]. For example, the absorption properties of TiO₂/Ag nanoparticle due to the LSPR effect excited on the Ag surface were examined and revealed for their application in solar energy harvesting reported by Xuan *et al* [10]. The He's group in Chen *et al.* [11] reported

* Corresponding author, e-mail: yuwei@sspu.edu.cn

that Au NP even at a very low concentration were effective for the solar light absorption. However, plasmonic NP with a single component are inclined to aggregate into less active sites after a long-time irradiation, which will weaken the light absorption gradually.

The Au-Pd alloy NP have been reported to effectively driven various reactions by the visible light, including the electrooxidation of methanol and formic acid, Suzuki-Miyaura cross coupling, oxidative addition of benzylamine, selective oxidation of aromatic alcohols, and *etc.* [12-15]. The Au-Pd NP-rGO (reduced graphene oxide) nanocomposite was reported to be a superior photo-thermal agent against cancer HeLa cells in comparison to monometallic Au and Pd NP counter parts [16]. Motivated by the previous results, it is anticipated that the Au-Pd alloy NP will exhibit better photo-thermal conversion than that of monometallic Pd or Au NP.

Furthermore, in comparison with pure plasmonic NP, the supported plasmonic NP have many advantages, which can not only enhance light absorption, but also separate from the fluids easily. So seeking for appropriate supported LSPR NP nanofluids is significant for the utilization of solar energy.

Carbon nanotubes are reported to be effective solar absorbers because of their high spectral absorptivity over the entire solar range [17]. The main difficulty in the large-scale use of carbon nanotubes nanofluids is the stability of the NP in suspension [18, 19]. It seems that nitrogen doping is an effective approach to improve the stability and dispersion of carbon nanotubes [20, 21]. Furthermore, chemical active sites induced by nitrogen atoms are favorable for the metal or metal oxide to anchor [22, 23]. So if the advantages of nitrogen doped carbon nanotubes and the Au-Pd alloy plasmonic NP can be combined together, the solar light absorption may be excellent. Inspired by these facts, we report a facile process to prepare Au-Pd NP supported on nitrogen-doped carbon nanotubes, which exhibits higher photo-thermal efficiency than that of pure nitrogen-doped carbon nanotubes and monometallic Pd or Au NP/N-CNTS under solar irradiation.

Experimental

Synthesis of N-CNT

All chemicals in the present work were purchased from Sinopharm Chemical Reagent Co. Ltd. Shanghai, China, and were used as received without further purification. The N-CNT were synthesized by a chemical vapor deposition according to our previous paper [21].

Synthesis of Au-Pd/N-CNT

The 15 wt.% Au-Pd/N-CNT nanofluids were prepared by polyethylene imine (PEI) reduction method. Typically, 0.2 g N-CNT powder were initially dispersed in 50-150 mL 1mol/L PEI solution by sonication for 30 min, then 13.2 mL 0.01 M HAuCl₄ and 3.76 mL 0.01 M H₂PdCl₄ aqueous solution were then added with vigorous stirring for 2 hour, then the solid was separated, washed with water and ethanol, and dried vacuum at 60 °C. For comparison, monometallic Pd/N-CNT and Au/N-CNT with the same loadings were also prepared using the similar procedures. All the nanofluids with the same concentration were dispersed in ethylene glycol (EG) by sonication for 30 min.

Characterization

The X-ray diffraction (XRD) patterns of the products were collected on a Bruker D8 ADVANCE instrument with Cu-K α radiation ($\lambda = 1.5418 \text{ \AA}$). The X-ray photoelectrospectroscopy (XPS) analysis were recorded on an Axis Ultra DLD instrument from Kratos, UK, using an Al K α X-ray radiation source at a power of 300 W. Scanning electron microscopy (SEM)

was carried out on Hitachi S-4800 with an acceleration voltage of 5 kV. Transmission electron microscopy (TEM) was performed on JEOL-JEM-1005 at 200 kV equipped with an energy dispersive X-ray (EDX) spectroscope. The specimens for TEM were prepared by suspending solid samples in ethanol with 15 min ultrasonication and placing a drop of this mixture on a 3.05 mm diameter copper mesh, which was then dried in air. Ultraviolet-visible-near infrared (UV-Vis-NIR) spectra of the NP and nanofluids were recorded on a Lambda 750 seconds spectrophotometer at room temperature.

Evaluation of the photo-thermal conversion properties

Graphic description of the photo-thermal conversion experimental system is shown and depicted in our previous paper [24]. Determination of the solar thermal utilization efficiency η is according to Chen *et al.* [25], that is $\eta = Q_{\text{NFS}}/I_0A$, Where I_0 is incident irradiance (1050 W m^{-2} in the current work) and A is the exposure area (4 cm^2 in the current work). The Q_{NFS} is the heat generation of the nanofluids, so the utilization efficiency $\eta = (T_{\text{eq}} - T_0)m_{\text{EG}}C_{\text{EG}}B/AI_0$, the constant B can be determined by plotting $\ln[T(t) - T_0]/(T_{\text{eq}} - T_0)$ vs. time, t . In these two equations, m_{EG} and C_{EG} is the mass and heat capacity components of the EG, respectively, T is the temperature, and t is time. The T_{eq} is the equilibrium temperature, T_0 is the ambient temperature.

Results and discussion

Characterization of Au-Pd/N-CNT

Figures 1(a)-1(c) show SEM images of bare N-CNT, fig. 1(a), and Au-Pd/N-CNT nanocomposites prepared with different PEI ratios. The results indicate that NP decorating on the surface of the N-CNT depends greatly on the PEI amount. There are scattered NP at PEI/NP = 50, fig. 1(b). Some NP aggregate in the solution with a small portion of NP deposited on N-CNT. When the PEI/NP ratio is 150, the size of NP on the surface of N-CNT is large. When the PEI/NP ratio is 100, the coverage of NP over the N-CNT surface is complete and uniform, suggesting that NP supported on N-CNT can be realized at an optimum PEI/NP ratio of 100. In this system, PEI acts as not only a stabilizing agent, but also a reducing agent, which could lead to uniform nucleation and growth of NP on the N-CNT surfaces. Low amount of PEI is insufficient for protecting or reducing the Pd(II) or Au(III) ions, leading to NP aggregates in the solution. Large amount of PEI would accelerate the reducing rate of Pd(II) or Au(III) ions, thus the nucleation growth rate is faster than nucleation itself, leading to uneven and large nanoparticles.

Figure 2 shows the XRD pattern of Au-Pd/N-CNT composite. From the figure, we can see the peak at 26.1° attribute to the (002) plane

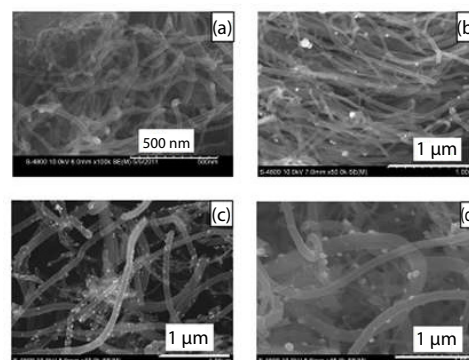


Figure 1. The SEM images of (a) bare N-CNT and 5 wt.% Au-Pd/N-CNT with (b) PEI: metal = 150:1 (c) PEI: metal = 100:1, and (d) PEI: metal = 50:1

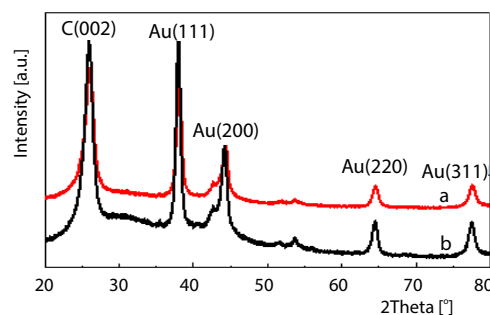


Figure 2. The XRD patterns of (a) 10 wt.% Au-Pd/N-CNT, and (b) 15 wt.% Au-Pd/N-CNT

of graphite in the N-CNT. Each XRD pattern showed four well resolved diffractions due to (111), (200), (220), and (311) diffractions of the face-centered cubic (fcc) structure of metallic Au and/or Pd, showing the existence of gold or Pd NP in the composite. The Pd peak is not obvious, which may due to that the Pd diffraction is overlapped with Au diffraction, because the Pd loading weight is much lower than the Au content.

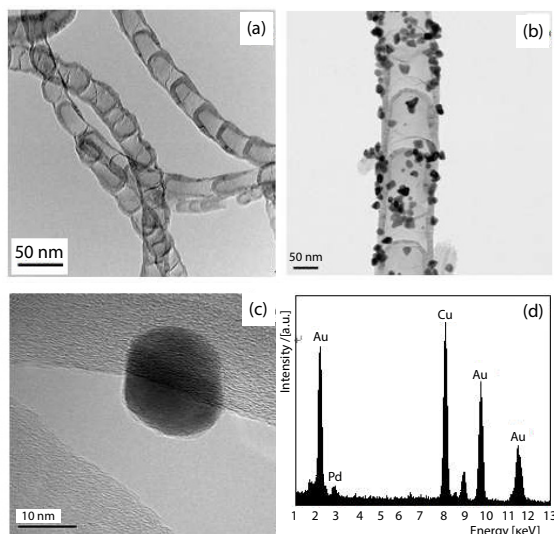


Figure 3. The TEM images of (a) bare N-CNT, (b) low-magnification TEM image, (c) high-magnification TEM image, and (d) EDS spectrum of 15 wt.% Au-Pd/N-CNT

The diameters of Au or Pd NP were in the range of 15-30 nm. The EDX further confirms the presence of Au and Pd in the Au-Pd/N-CNT nanocomposites, fig. 3(d). The Cu signal originates from the copper mesh.

Figure 3 shows the TEM images of the bare N-CNT and the 15 wt.% Au-Pd/N-CNT composite. The N-CNT is composed of individual nanobamboo stacked together to form the long nanofibers with a clear, smooth surface. It is clearly observed that for Au-Pd/N-CNT, the surface of the bamboo-like morphology of N-CNT is entirely covered by Au or Pd NP, figs. 3(b) and 3(c). The diameters of Au or Pd NP were in the range of 15-30 nm. The EDX further confirms the presence of Au and Pd in the Au-Pd/N-CNT nanocomposites, fig. 3(d). The Cu signal originates from the copper mesh.

The atomic Au/Pd ratios detected from XPS are 8.07 for the samples, suggesting that the surfaces of the Au-Pd/N-CNT samples are enriched with Au. The binding energies at 84.0 and 87.6 eV are ascribed to Au 4f_{7/2} and Au 4f_{5/2}, respectively, which are consistent with zerovalent Au [26], fig. 4(a). The XPS peaks of Pd NP is not very obvious due to its low mass loadings. But it still can be seen that the binding energies at 340.9 and 335.5 eV are assigned to Pd 3d_{3/2} and Pd 3d_{5/2}, respectively, fig. 4(b). These results confirmed that the Au-Pd alloy NP are supported on the surface of N-CNT.

The atomic Au/Pd ratios detected from XPS are 8.07 for the samples, suggesting that the surfaces of the Au-Pd/N-CNT samples are enriched with Au. The binding energies at 84.0 and 87.6 eV are ascribed to Au 4f_{7/2} and Au 4f_{5/2}, respectively, which are consistent with zerovalent Au [26], fig. 4(a). The XPS peaks of Pd NP is not very obvious due to its low mass loadings. But it still can be seen that the binding energies at 340.9 and 335.5 eV are assigned to Pd 3d_{3/2} and Pd 3d_{5/2}, respectively, fig. 4(b). These results confirmed that the Au-Pd alloy NP are supported on the surface of N-CNT.

The optical properties of Au-Pd/N-CNT nanofluids

The optical properties of the nanofluids have significant effect on the solar photo-thermal conversion. So the optical absorbance of different nanofluids was measured using a

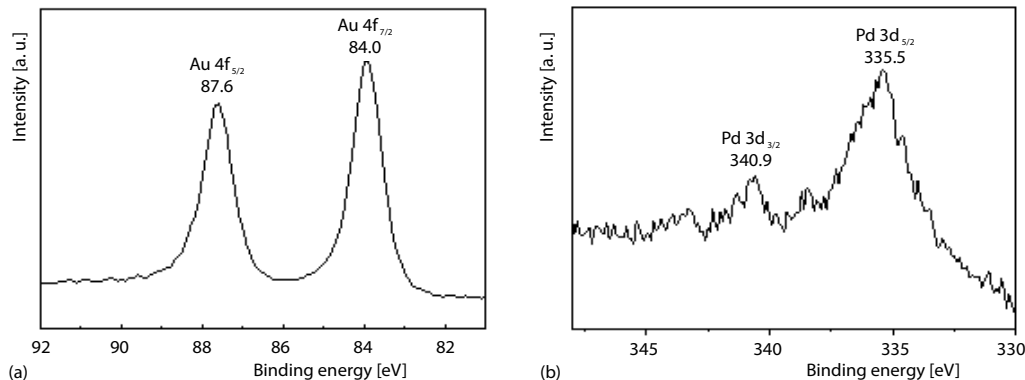


Figure 4. The XPS spectra of (a) Au 4f, and (b) Pd 3d regions for 15 wt.% Au-Pd/N-CNT

UV-Vis-NIR spectrum, which is shown in fig. 5(a). Compared with base EG liquid, all N-CNT-based nanofluids show a broadband absorption across the visible region and near-infrared region, as also found for multi-walled carbon nanotubes [27], which can be attributed to 1-D van Hove singularities [19]. It was actually observed that the transmittance decreased in the order EG < N-CNT < Pd/N-CNT < Au/N-CNT < Au-Pd/N-CNT. Furthermore, there is no obvious Au or Pd NP absorption peak due to the strong adsorption of carbon nanotubes.

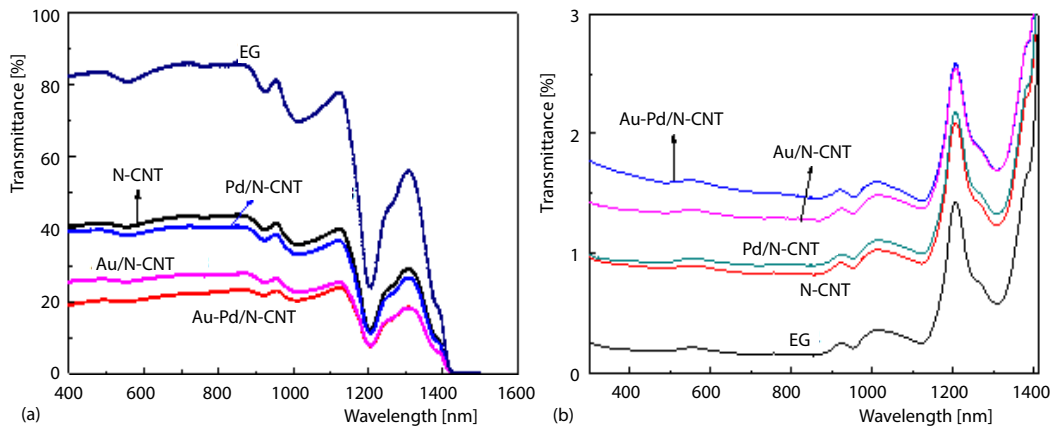


Figure 5. The UV-Vis-NIR spectra (a) and the extinction coefficients of EG and different N-CNT-based nanofluids (b)

According to the relationship between the absorbance and the concentration by the Beer-Lambert law, extinction coefficient $a(\lambda)$ can be calculated according to $T(\lambda) = \exp[-a(\lambda)L]$ where L is the length of light crossing and it is 10 mm, $T(\lambda)$ is transmittance coefficient. The extinction coefficient of N-CNT-based nanofluids is shown in fig. 5(b).

The Au-Pd/N-CNT nanofluids give the highest $a(\lambda)$ in the solar illumination region reasonably, indicating the highest absorption of solar illumination among N-CNT, Au/N-CNT, and Pd/N-CNT nanofluids.

According to the extinction coefficient of the nanofluids, a solar spectrum-weighted stored energy fraction, A_m , can be calculated from Drotning [28]:

$$A_m = \frac{\int_{\lambda_{\min}}^{\lambda_{\max}} I(\lambda)(1 - e^{-a(\lambda)l})d\lambda}{\int_{\lambda_{\min}}^{\lambda_{\max}} I(\lambda)d\lambda}$$

where $I(\lambda)$ is the spectral solar irradiance, $a(\lambda)$ – the absorption coefficient, and l – the penetration distance. The term $I(\lambda)(1 - e^{-a(\lambda)l})$ in the equation represents the solar energy absorbed by nanofluids at a penetration distance of l cm and a given wave length of λ . In comparison with base EG fluid, the curves of $I(\lambda)(1 - e^{-a(\lambda)l})$ for all the N-CNT-based nanofluids come close to the curve of the spectral solar irradiance $I(\lambda)$ (ASTM G173-03 AM 1.5 Global). The nearer to $I(\lambda)$, the more solar irradiation absorbed by the nanofluids. So the Au-Pd/N-CNT nanofluids may absorb the most solar irradiation among these nanofluids.

After integrating $I(\lambda)(1 - e^{-a(\lambda)l})$ and $I(\lambda)$ in fig. 6(a), A_m of the nanofluids can be determined from the previous equation using a base fluid EG as a reference, which is shown in fig. 6(b). The penetration distance affect the A_m of the nanofluids obviously. The A_m increased

rapidly with the penetration distance at the beginning, and then slowed down as the penetration distance increase gradually. The A_m reached 79.7% and 60.4% at the penetration distance of 1 cm for Au-Pd/N-CNT nanofluids and N-CNT, respectively, and finally about 90% at 2 cm for all the N-CNT-based nanofluids. With the same A_m , the penetration distance decrease in the order EG > N-CNT > Pd/N-CNT > Au/N-CNT > Au-Pd/N-CNT.

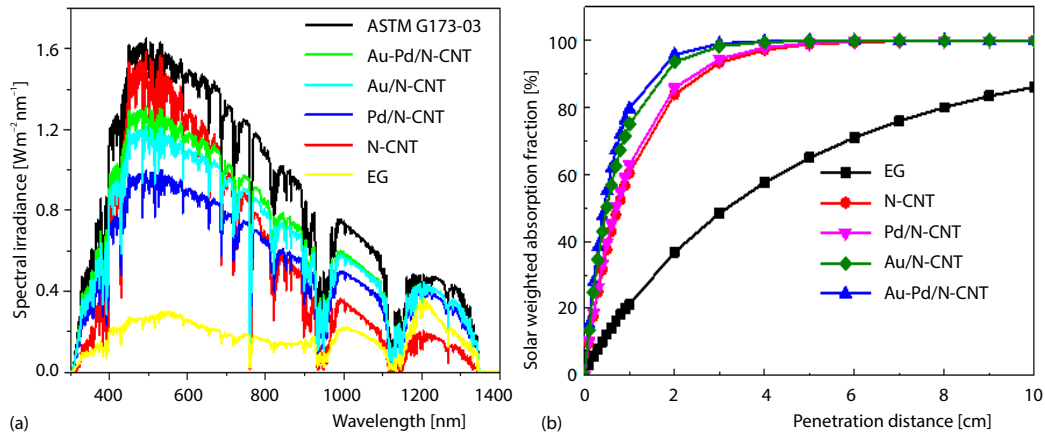


Figure 6. Spectral irradiance ASTM G173-03 and the term $I(\lambda)(1-e^{-u(\lambda)})$ (a) dependence of A_m and penetration distance of of EG and different N-CNT based nanofluids (b)

Photo-thermal conversion properties of N-CNT-based nanofluids

The different N-CNT-based nanofluids were irradiated by a simulated solar light under a solar flux of $1050 W/m^2$. The irradiation time had a great effect on the temperature rise. The temperature increased rapidly with the irradiation time at the beginning, and then slowed down as the heat dissipation played the major role. Then the temperature reached an equilibrium value for 10800 s at which the heat dissipation rate is equal to the heat generation rate. After that the solar simulator was shut down and the nanofluids were cooled to the ambient temperature. The curves of the temperature rise of the nanofluids were presented in fig. 7(a). It was actually observed that temperature rise of nanofluids obviously decreased in the order EG < N-CNT < Pd/N-CNT < Au/N-CNT < Au-Pd/N-CNT, which is consistent with the optical absorbance. The maximal temperature rise could reach $43.5^\circ C$ for Au-Pd/N-CNT nanofluids, while $36.6^\circ C$ and $31.8^\circ C$ for N-CNTs and EG, respectively. It is worth noting that the temperature increment of Au-Pd/N-CNT nanofluids is more obvious than that of monometallic Pd/N-CNT or Au/N-CNT.

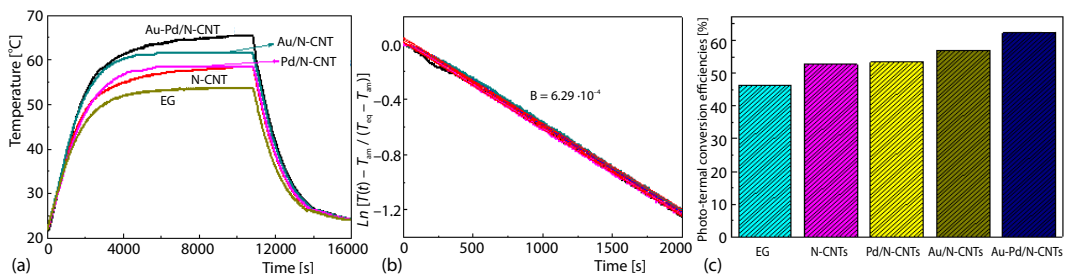


Figure 7. Temperature rise; (a) EG and different N-CNT-based nanofluids, (b) the plotting of $\ln(\Delta T/\Delta T_{c0})$ vs. time t in the cooling stage, and (c) the solar utilization efficiencies of EG and different N-CNT-based nanofluids

The photo-thermal conversion efficiency of the nanofluids is shown in fig. 7(c), the quantification is according to the method [24, 25]. Firstly, the constant B is determined by plotting $\ln[T(t)-T_0]/(T_{\text{eq}}-T_0)$ vs. time t , which is presented in fig. 7(b). The constant B is $6.29 \cdot 10^{-4} \text{ s}^{-1}$ in our current experimental system, then the efficiency can be obtained accordingly. The efficiency of base fluid EG is 46.3%, which is lower than N-CNT-based fluids. It was clearly observed that the efficiency increased in the order of Au-Pd/N-CNT > Au/N-CNT > Pd/N-CNT, with the same tendency as the solar spectrum-weighted stored energy fraction.

Conclusion

In summary, Au-Pd alloy NP have been decorated successfully on the N-CNT surfaces using a PEI reduction method. The optical properties of N-CNT-based fluids were investigated in detail. The photo-thermal conversion efficiency of Au-Pd/N-CNT nanofluids is superior to that of monometallic Pd/N-CNT and Au/N-CNT nanofluids, with the same tendency as the solar weighted absorption fractions. Further investigation on the optical and photo-thermal conversion properties of Au-Pd alloy nanofluids with different ratios and different shapes is underway.

Acknowledgment

This work was supported by National Natural Science Foundation of China (51476094 and 51590900), Shanghai Municipal Natural Science Foundation (Grant No. 17ZR1411000) and the Key Subject of Shanghai Polytechnic University (Material Science, XXKPY1302, and A01GY17F022).

References

- [1] Lefebvre, D., Tezel, F. H., A Review Energy Storage Technologies with a Focus on Adsorption Thermal Energy Storage Processes for Heating Applications, *Renewable & Sustainable Energy Reviews*, 67 (2017), Jan., pp. 116-125
- [2] Shannon, M. A., Science and Technology for Water Purification in the Coming Decades, *Nature*, 452 (2008), Mar., pp. 301-310
- [3] Narayan, G. P., The Potential of Solar-Driven Humidification-Dehumidification Desalination for Small-Scale Decentralized Water Production, *Renewable & Sustainable Energy Reviews*, 14 (2010), 4, pp. 1187-1201
- [4] Das, S. K., *et al.*, *Nanofluids: Science and Technology*, John Wiley & Sons Inc., New York, USA, 2007
- [5] Choi, S., *et al.*, Enhancing Thermal Conductivity of Fluids with Nanoparticles, Developments and Applications of Non-Newtonian Flows, *ASME*, 231 (1995), 66, pp. 99-105
- [6] Baffou, G., Quidant, R., Thermo-Plasmonics: Using Metallic Nanostructures as Nano-Sources of Heat, *Laser Photonics Reviews*, 7 (2013), 2, pp. 171-187
- [7] Baffou, G., *et al.*, Nanoscale Control of Optical Heating in Complex Plasmonic Systems, *ACS Nano*, 4 (2010), 2, pp. 709-716
- [8] Pinchuk, A., *et al.*, Influence of Interband Electronic Transitions on the Optical Absorption in Metallic Nanoparticles, *Journal of Physics D: Applied Physics*, 37 (2004), Oct., pp.3133-3139
- [9] Yamada, K., *et al.*, Thermionic Emission of Electrons from Gold Nanoparticles by Nanosecond Pulse-Laser Excitation of Interband, *Journal of Physical Chemistry C*, 111 (2007), 30, pp. 11246-11251
- [10] Xuan, Y. M., *et al.*, Enhancement of Solar Energy Absorption using a Plasmonic Nanofluid based on TiO₂/Ag Composite Nanoparticles, *RSC Advances*, 4 (2014), 31, pp. 16206-16213
- [11] Chen, M. J., *et al.*, Enhancement of Photothermal Conversion using Gold Nanofluids with Different Particle Sizes, *Energy Conversion and Management*, 112 (2016), Mar., pp. 21-30
- [12] Horinouchi, S., *et al.*, Hydrogen Storage Properties of Isocyanide-Stabilized Palladium Nanoparticles, *Langmuir*, 22 (2006), 4, pp. 1880-1884
- [13] Harpeness, R., Gedanken, A., Microwave Synthesis of Core-Shell Gold/Palladium Bimetallic Nanoparticles, *Langmuir*, 20 (2004), 8, pp. 3431-3434

- [14] Chen, X., AuPd Bimetallic Nanoparticles Decorated on Graphene Nanosheets: Their Green Synthesis, Growth Mechanism and High Catalytic Ability in 4-Nitrophenol Reduction, *Journal of Materials Chemistry A*, 2 (2014), 16, pp. 5668-5674
- [15] Sarina, S., *et al.*, Enhancing Catalytic Performance of Palladium in Gold and Palladium Alloy Nanoparticles for Organic Synthesis Reactions through Visible Light Irradiation at Ambient Temperatures, *Journal of the American Chemical Society*, 135 (2013), 15, pp. 5793-5801
- [16] Darabdhara, G., *et al.*, Reduced Graphene Oxide Nanosheets Decorated with AuPd Bimetallic Nanoparticles: A Multifunctional Material for Photothermal Therapy of Cancer Cells, *Journal of Materials Chemistry B*, 3 (2015), 42, pp. 8366-8374
- [17] Taylor, R. A., *et al.*, Nanofluid Optical Property Characterization: towards Efficient Direct Absorption Solar Collectors, *Nanoscale Research Letters*, 6 (2011), 1, pp. 225-236
- [18] Taylor, R. A., *et al.*, Small Particles, Big Impacts: A Review of the Diverse Applications of Nanofluids, *Journal of Applied Physics*, 113 (2013), 1, pp. 011301-1-19
- [19] Yu, W., Xie, H., A Review on Nanofluids: Preparation, Stability Mechanisms, and Applications, *Journal of Nanomaterials*, 2012 (2012), ID435873
- [20] Lee, J. M., *et al.*, Selective Electron-or Hole-Transport Enhancement in Bulk-Heterojunction Organic Solar Cells with N-or B-Doped Carbon Nanotubes, *Advanced Materials*, 23 (2011), 5, pp. 629-633
- [21] Wang, L. L., *et al.*, Nitrogen-Doped Carbon Nanotubes with Variable Basicity: Preparation and Catalytic Properties, *Catalysis Communications*, 15 (2011), 1, pp. 78-81
- [22] Park, J. S., *et al.*, A ZnO/N-Doped Carbon Nanotube Nanocomposite Charge Transport Layer for High Performance Optoelectronics, *Journal of Materials Chemistry*, 22 (2012), 25, pp. 12695-12700
- [23] Wang, L. L., *et al.*, Facile Green Synthesis of Pd/N-Doped Carbon Nanotubes Catalysts and their Application in Heck Reaction and Oxidation of Benzyl Alcohol, *Journal of Physics and Chemistry of Solids*, 107 (2017), Aug., pp. 125-130
- [24] Wang, L. L., *et al.*, Photothermal Properties of Near-Spherical Gold Nanofluids with Strong Localized Surface Plasmon Resonance, *Journal of Thermal Science and Engineering Applications*, 10 (2018), 1-5, pp. 011015
- [25] Chen, N., *et al.*, Complementary Optical Absorption and Enhanced Solar Thermal Conversion of CuO-ATO Nanofluids, *Solar Energy Materials & Solar Cells*, 162 (2017), Apr., pp. 83-92
- [26] Turcheniuk, K., *et al.*, Plasmonic Photothermal Destruction of Uropathogenic *E. Coli* with Reduced Graphene Oxide and Core/Shell Nanocomposites of Gold Nanorods/Reduced Graphene Oxide, *Journal of Materials Chemistry B*, 3 (2015), 3, pp. 375-38
- [27] Hordy, N., *et al.*, High Temperature and Long-Term Stability of Carbon Nanotube Nanofluids for Direct Absorption Solar Thermal Collectors, *Solar Energy*, 105 (2014), July, pp. 82-90
- [28] Drotning, W. D., Optical Properties of Solar-Absorbing Oxide Particles Suspend in a Molten Salt Heat Transfer Fluid, *Solar Energy*, 20 (1978), 4, pp. 313-319